

PHYSICAL EVALUATION OF FDM-PRINTED CARBON FIBER REINFORCED PLA: MECHANICAL STRENGTH, MOISTURE SENSITIVITY, AND POROSITY

M. DHOUIOUI¹, W. ZGHAL², H. HENTATI^{1,3*}, B. BEN FRAJ⁴, M. BEN AMAR⁵, M. HADDAR¹

¹ LA2MP Laboratory, University of Sfax, Tunisia

E-mail: dhouiouimanel7@gmail.com E-mail: mohamed.haddar2016@gmail.com

² High institute of Industrial Management of Sfax, University of Sfax, Tunisia

E-mail: wissem.zghal@isgis.usf.tn

³ ESSTHS, University of Sousse, Tunisia

E-mail: hamdi.hentati@yahoo.fr

⁴ Nanomaterials and Systems for Renewable Energy Laboratory, Research and Technology Center of Energy, Technopole Borj Cedria, Hammam Lif, Tunisia

E-mail: boutheina.benfracj2024@gmail.com

⁵ Laboratoire des Sciences des Procédés et des Matériaux, CNRS, Université Sorbonne Paris Nord, Villetaneuse, France

E-mail: mounir.benamar@lspm.cnrs.fr

Abstract. This study investigates the physical properties of short carbon fiber reinforced poly(lactic acid) (SCFR-PLA) specimens produced by fused deposition modeling (FDM). The influence of fiber content, raster angle, and printing speed on mechanical, hygroscopic, and microstructural behavior is analyzed. Printing at a 0° raster angle provides maximum stiffness and tensile strength, while higher speeds enhance strength and ductility but reduce stiffness. Carbon fiber addition improves stiffness, strength, and moisture resistance. SEM analysis reveals pore morphology, linking porosity to mechanical and hygroscopic variations. Correlations among fiber–matrix adhesion, voids, moisture uptake, and durability are also discussed.

Key words: Porosity, SEM observations, hygroscopic properties, FDM process, SCFR-PLA.

1. INTRODUCTION

Various studies have advanced the damage characterization of various materials through combined experimental and numerical approaches [1–3]. Moreover, understanding how manufacturing parameters influence both microstructure and structural integrity is essential for optimizing physical properties and enhancing component performance [4–6]. In recent years, growing interest in additive manufacturing has driven extensive research into the physical characterization and interrelationships

between mechanical behavior and microstructural features of polymer-based composites. 3D printing with thermoplastic polymers is currently widely used in prototyping and modeling. In the context, current research focuses on material performance, while exploiting advanced manufacturing techniques to improve mechanical and functional properties. Scientists use experimentation and numerical modeling to understand the behavior of printed composite parts from molecular to macroscopic scales [7,8]. Among the commonly used 3D printing processes for prototyping and part production, fused deposition modeling (FDM) is recognized for its cost-effectiveness and high printing speeds for polymer composites compared to other 3D printing techniques [9,10].

Le et al. [11] demonstrated that incorporating MWCNTs into ABS filaments improves tensile strength and modifies melt flow, with DSC and MFI analyses revealing property changes that directly affect the mechanical performance and thermal behavior of FDM-printed parts. Ferreira et al. [12] have characterized 3D printed materials, focusing on PETG thermoplastic with and without short fiber reinforcement. This study highlights how FDM parameters and fiber content influence the thermal stability, mechanical performance, and microscopic characteristics of the printed parts. Juan et al. [13] have explored a structural composite consisting of 3D printed continuous carbon fiber reinforced polylactic acid (CCFR-PLA) for hip prosthetic implants. Thermal and structural characterizations revealed chemical interactions between PLA and carbon fiber, influencing thermal properties. The studied composite exhibited high cell viability and physical properties comparable to bone, suggesting its potential suitability for femoral stem prostheses in orthopedic applications.

Our focus in this paper is on exploring the behavior of short carbon fiber reinforced PLA (SCFR-PLA) composites produced by the FDM process. In this context, PLA, a semi-crystalline polymer, is considered as the best thermoplastics for 3D printing [14,15]. Its features include flexibility, high tensile strength, and relatively lower flexural strength compared to other polymers [16-18]. Hsueh et al. [19] have investigated PLA and PETG materials printed by the FDM technique under different loading conditions and printing parameters. Their study revealed that higher printing temperatures improved the mechanical properties of both materials. PLA showed superior mechanical strength compared to PETG, while PETG exhibited lower thermal deformation, offering valuable insights for optimizing polymer-based FDM applications.

The addition of carbon fibers to these printed polymers ameliorates considerably their mechanical and thermal behaviors. In fact, the physical properties of SCFR-PLA can be affected by several factors related to its composition and the selected 3D printing parameters. Maqsood and Rimasauskas [20] have examined the mechanical and fracture behaviors of 3D-printed materials, including pure PLA, SCFR-PLA, and CCFR-PLA. It was found that vacuum printing provides enhanced mechanical properties compared to atmospheric printing. This improvement is attributed to a reduction in porosity within the printed part [21]. The investigation was also extended to explore the effect of annealing at various temperatures on the thermal, tensile, and microstructural properties of both pure PLA and SCFR-PLA [22]. It was shown that the annealing process significantly affects the crystallinity of the tested materials. Crystallinity increases with rising annealing temperatures, with no notable effect on the mechanical properties of SCFR-PLA.

The aim of this research work is to investigate the correlations between mechanical behavior, water absorption, porosity, and microstructural features of FDM-printed PLA and SCFR-PLA, in order to assess the effect of carbon fiber content and printing parameters on their physical properties. The obtained results are supported by scanning electron microscopy (SEM) observations, highlighting the microstructural behaviors of composite parts printed under various printing speeds.

2. MATERIALS AND METHODS

Following the ASTM D638 standard, FDM technology was employed to print the tensile specimens on pure PLA and SCFR-PLA. The fixed printing settings used

were as follows: filament diameter of 1.75 ± 0.05 mm, 100% infill percentage, extrusion width of 1.28 mm, extrusion temperature of 210 °C, and layer thickness of 0.4 mm. Diverse printing parameters were selected which are three raster angles (θ), two distinct printing speeds (V) and three carbon fiber contents (%C). The details of these selected variables are presented in the Table 1.

Table 1
Variable FDM printing parameters

| 3D printing settings | | %C (%) |
|----------------------|----------|-------------|
| θ (°) | V (mm/s) | |
| 0 – 45 – 90 | 25 – 50 | 0 – 15 – 30 |

A full factorial experimental design was adopted to investigate the influence of FDM parameters on the mechanical, hygroscopic, and microstructural properties of printed specimens. Three materials were selected: pure PLA, PLA reinforced with 15 wt% short carbon fibers (PLA-15%C), and PLA reinforced with 30 wt% short carbon fibers (PLA-30%C). Each material was printed using three raster angles (0°, 45°, and 90°) and two printing speeds (25 mm/s and 50 mm/s), resulting in a total of 18 distinct configurations. For each configuration, two identical specimens were produced for every test type. This experimental matrix was applied to tensile testing, moisture absorption measurements, and porosity analysis. The design ensured that the main effects and interactions of the selected parameters could be quantitatively assessed. To explore the effect of these printing parameters on the mechanical properties of the printed samples were subjected to uniaxial tensile test until failure at room temperature. An extensometer was used in each tensile test to accurately measure the strain of the examined parts. Mechanical properties were determined from the stress-strain curves. In addition, to investigate the water uptake behavior of the PLA-based composite materials, all specimens were thoroughly dried and weighed to determine their initial dry mass prior to immersion (m_0). The samples were then fully immersed in distilled water maintained at 25 °C for various immersion periods. At specific time intervals (3, 7, and 30 days), the specimens were removed, smoothly wiped to eliminate surface moisture, and weighed again (m_t). The percentage of water absorbed was calculated using the equation:

$$\text{Water Absorption}(\%) = \left(\frac{m_t - m_0}{m_0} \right) \times 100 \quad (1)$$

These mass are measured over time during immersion. This methodology enabled the evaluation of how material composition, layer orientation, and FDM processing parameters influence water absorption behavior. Furthermore, porosity (Pt) was determined allowing the estimation of total void content, providing a link between processing parameters and the formation of internal defects. Then, scanning electron microscopy (SEM-QUANTA FEG-250) was used to examine the

microstructural behavior of the tensile fractured surfaces. Porosity is equal to pore volume (V_P) divided by total volume (V_t). It is expressed by equation 2:

$$Pt = \frac{V_P}{V_t} = \left(\frac{M_t - M_s}{M_t} \right) \quad (2)$$

Where M_t is the dry mass of the specimen measured in air, and M_s is the saturated mass after immersion in water, allowing complete filling of the open pores. The difference ($M_t - M_s$) represents the mass of water occupying the accessible pores, which is directly proportional to the pore volume. Dividing this value by M_t normalizes the pore content with respect to the specimen's total volume, thus providing a dimensionless measure of porosity.

3. EXPERIMENTAL TENSILE RESULTS

Samples of tensile stress-strain curves of SCFR-PLA printed parts for various carbon fiber contents (%C), raster angles (θ) and printing speeds (V) are illustrated in Figure 1.

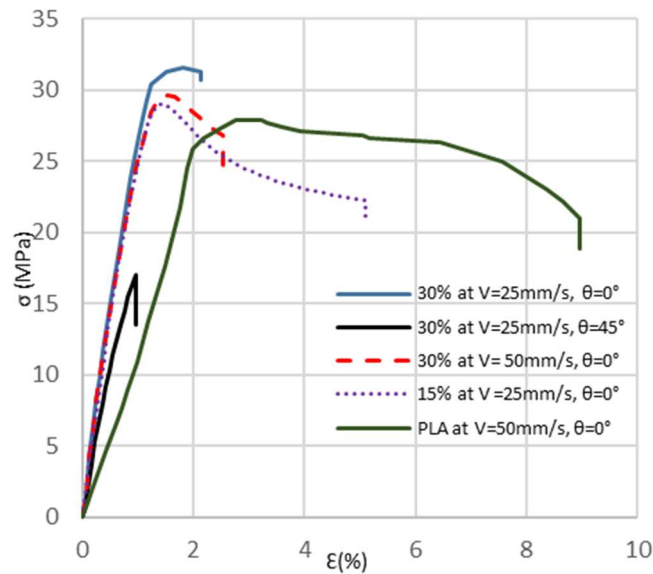


Fig. 1 – Tensile stress-strain curves of SCFR-PLA at different FDM parameters.

The variation of FDM parameters significantly affect the mechanical behavior and damage of printed parts. Therefore, it is interesting to explore their influence on measured mechanical properties, which are Young's modulus (E), ultimate tensile strength (UTS), yield strength (YS) and strain at failure (ϵ_f).

3.1. EVOLUTION OF YOUNG'S MODULUS

Figure 2 illustrates the variation of E as a function of θ , V and %C.

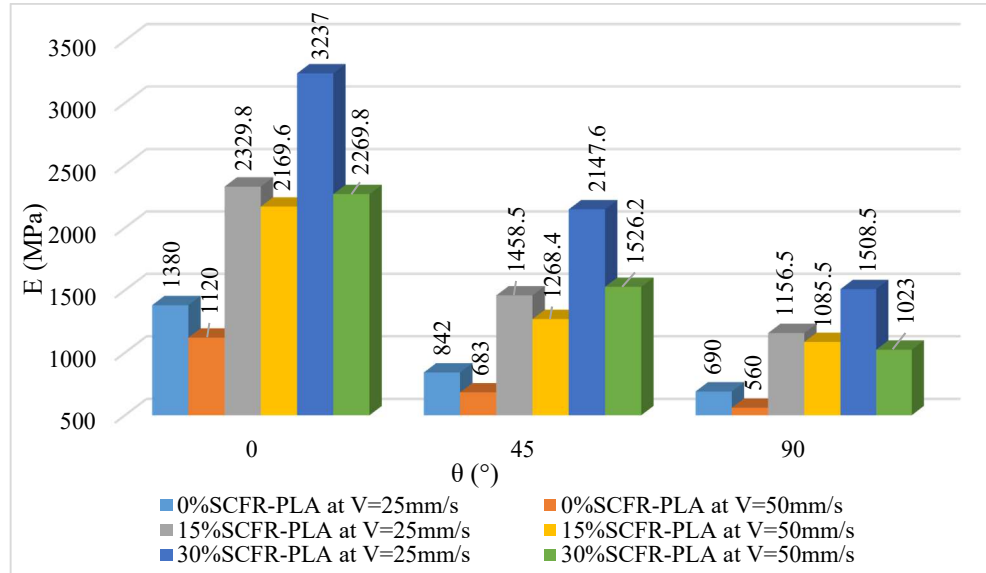


Fig. 2 – Variation of E with different values of θ , V, and %C.

Figure 2 illustrates a decrease in E with increasing θ and V, indicating a reduction in stiffness. The highest stiffness was observed at $\theta=0^\circ$, demonstrating the best rigidity. A similar pattern was reported by Ammar et al. [23] for carbon fiber-reinforced PETG. Furthermore, the addition of short carbon fibers significantly increases the stiffness of the material. This improvement is attributed to the reinforcing effect of the short carbon fibers, which enhance the structural integrity and mechanical properties of the printed material [25,26]. Furthermore, for $\theta=0^\circ$, the 30%SCFR-PLA, printed at low printing speed ($V=25\text{mm/s}$), exhibits the highest E value ($E=3237\text{ MPa}$). An analysis of the results reveals that the rigidity exhibits an inverse relationship with θ and V, while it increases proportionally with the carbon fiber content (%C).

3.2. EVOLUTION OF YIELD STRENGTH

The variation of YS as a function of FDM parameters is presented in Figure 3. The results indicate that YS decreases by approximately 65% as θ increases from 0° to 90° , specifically for %C=15% in SCFR-PLA printed at $V=50\text{ mm/s}$. Furthermore, an increase in %C from 15% to 30% enhances YS, especially at raster angles $\theta=45^\circ$ and $\theta=90^\circ$. In this case, printing speed has not a significant effect on YS.

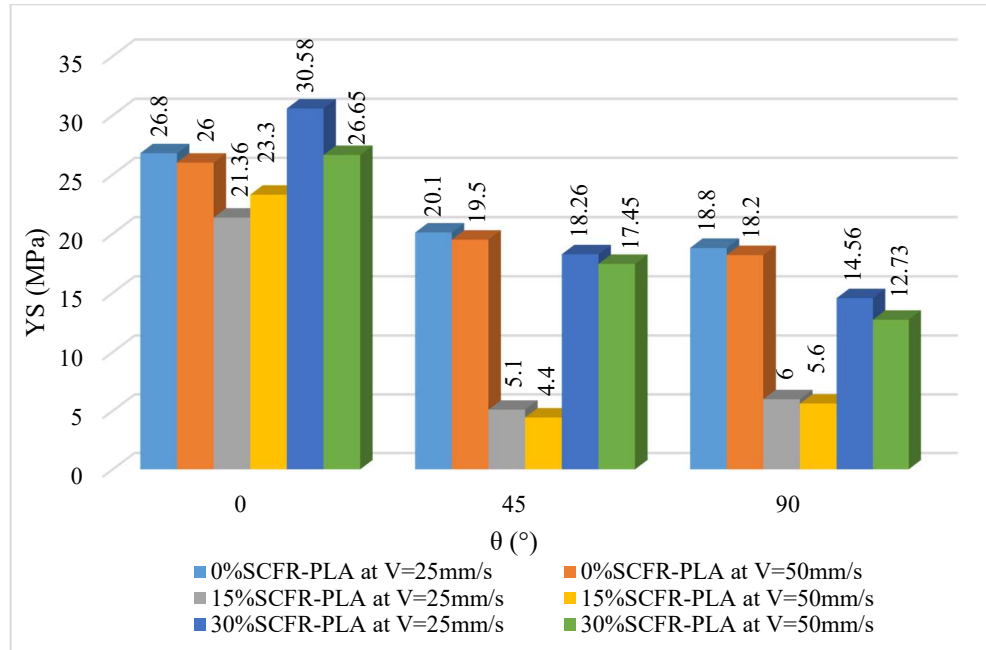


Fig. 3 – Variation of YS with different values of θ , V , and %C.

In addition, this figure shows a consistent decrease in YS with an increase in %C from 0% to 15%, respectively. This trend is attributed to the reduction in elasticity of the pure polymer matrix caused by carbon fiber reinforcement [30]. The obtained results clearly show an inverse proportional relationship between YS and θ , and %C, with no notable influence of V .

3.3. EVOLUTION OF ULTIMATE TENSILE STRENGTH

Figure 4 illustrates the variation of UTS as a function of θ , V and %C. A significant 75% decrease in UTS as θ increases from 0° to 90° for %C = 15% and $V = 50$ mm/s. The influence of V is minimal for samples printed at 0° , whereas for those printed at 45° and 90° , an increase in V is observed to enhance UTS. This effect occurs because, at higher printing speeds, successive layers are deposited in shorter time intervals compared to lower speeds, promoting stronger interlayer bonding and improving the overall structural integrity of the printed material. This phenomenon was also demonstrated by Ansari and Kamil [27] for printed PLA. Furthermore, for the raster angles, 45° and 90° , we note that the increase of %C from 15% to 30% improves the tensile strength of the printed parts. The impact of %C is emphasized, indicating that incorporating carbon fiber into the PLA matrix leads to

an increase in UTS, thereby enhancing durability and toughness of the printed composites under tensile loading.

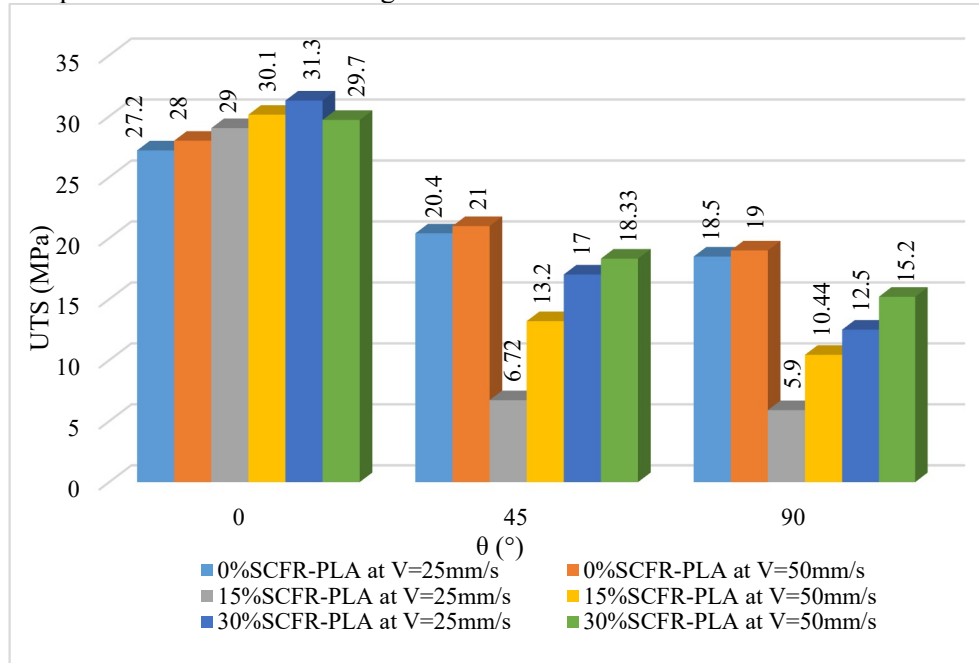


Fig. 4 – Variation of UTS with different values of θ , V, and %C.

Then, UTS decreases with increasing θ and while it increases proportionally with V and %C.

3.4. EVOLUTION OF STRAIN AT FAILURE

The ductility of the printed polymer and its composites is evaluated based on the fracture strain (ϵ_f) obtained from tensile testing. Figure 5 presents the variation of ϵ_f as a function of key FDM processing parameters, providing insights into how these factors influence the material's deformation ability before failure.

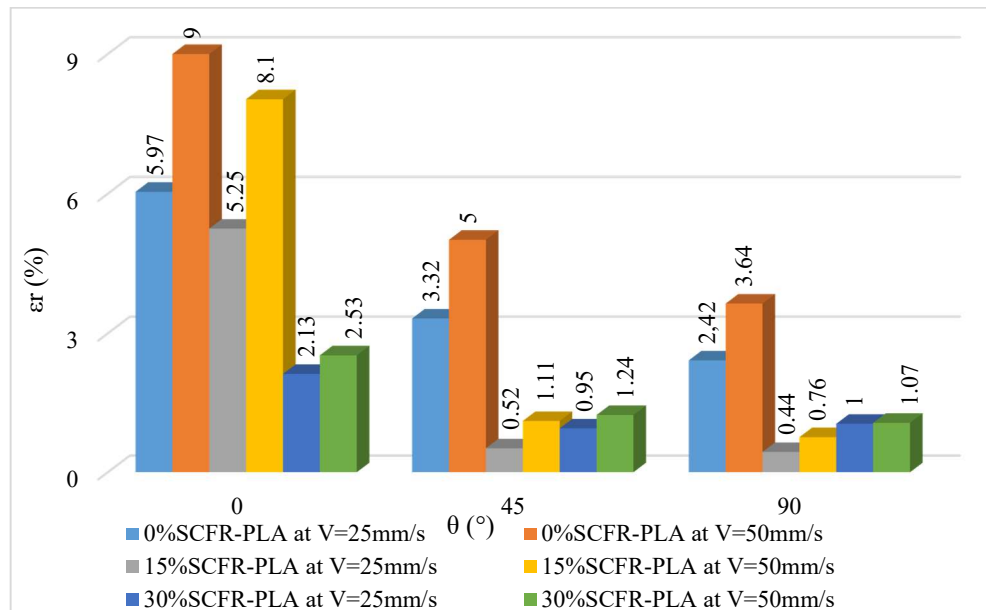


Fig. 5 – Variation of ϵ_f (%) with different values of θ , V , and %C.

The strain at failure is strongly affected by θ and V . Notably, low %C parts printed at 0° at high speed exhibit higher ductility compared to the other samples, with a corresponding ϵ_f reaching 9%. On the other hand, by changing θ from 0° to 90° , ϵ_f drops by about 90%, in the case of %C=15% printed at 50mm/s.

In addition, Figure 5 demonstrates that pure PLA exhibits superior ductility compared to the 15% carbon fiber reinforced PLA, regardless of the selected printing speed (V). These findings are in strong agreement with those reported in previous studies [20,25], further validating the outcome observed in the current analysis.

4. WATER ABSORPTION OF SCFR-PLA

The experimental outcomes provide valuable insight into the moisture sensitivity of SCFR-PLA composites and help relate water uptake to porosity, fiber-matrix interfacial bonding, and overall microstructural characteristics of FDM-printed parts.

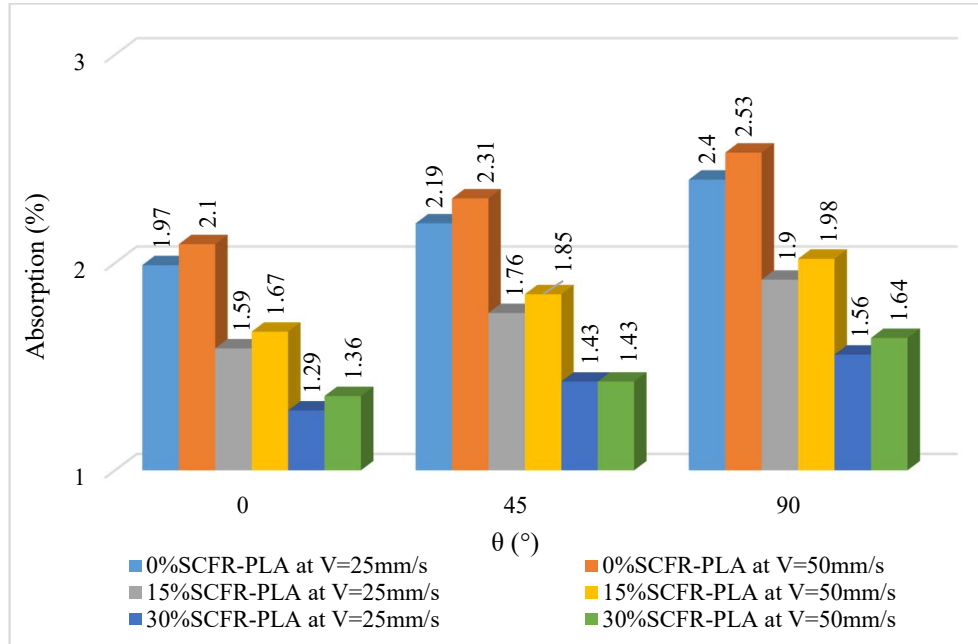


Fig. 6 – Influence of FDM parameters on materials absorption.

Figure 7 illustrates the mean values of the water absorption behavior of pure PLA and its composites with 15% and 30% short carbon fiber reinforcement (SCFR-PLA) over 3, 7, and 30 days. For each material, the average water absorption is calculated as:

$$\bar{A}_t = \frac{1}{n} \sum_{i=1}^n A_{i,t} \quad (3)$$

Where:

- \bar{A}_t = average water absorption (%) at time t for a specific material.
- $A_{i,t}$ = water absorption value of the i-th sample of that material at time t.
- n = total number of tested samples for that material at time t.

A clear trend is observed: water absorption increases with time for all materials, but decreases as the carbon fiber content increases. Pure PLA exhibits the highest absorption values at all time intervals, while the 30% SCFR-PLA composite consistently shows the lowest. This indicates that the addition of carbon fibers improves the material's resistance to moisture uptake, likely due to their hydrophobic nature and the reduced exposure of the polymer matrix.

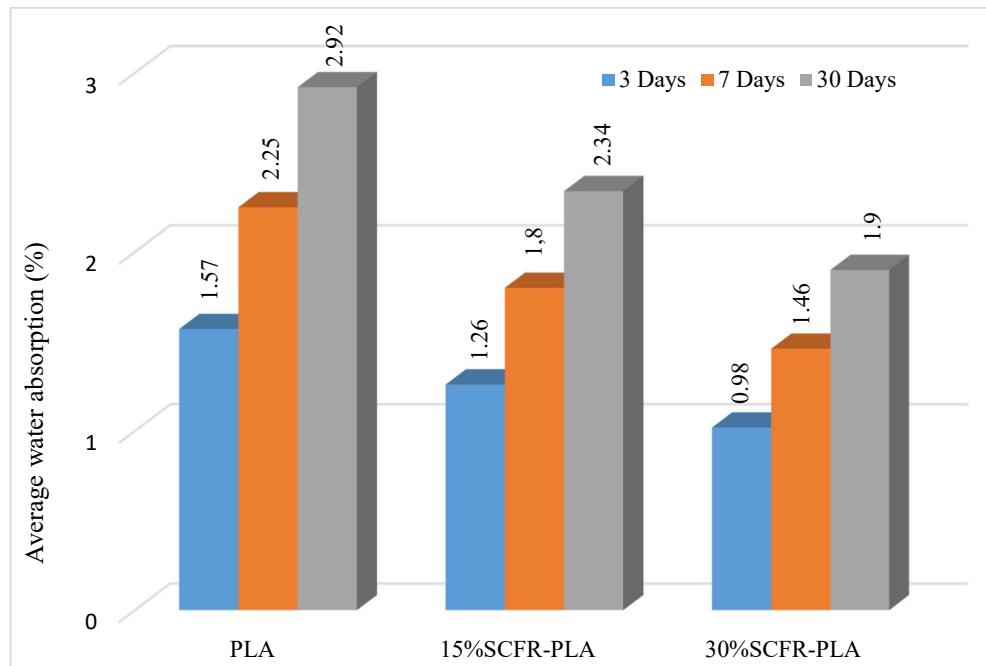


Fig. 7 – Mean values of materials water absorption as function of days.

The resulting averages were 2.25% for PLA, 1.8% for 15% SCFR-PLA, and 1.46% for 30% SCFR-PLA. Then, increasing the carbon fiber content effectively enhances the moisture resistance of the composite. In addition, the water absorption results over 3, 7, and 30 days reveal that increasing %C in SCFR-PLA composites significantly reduces both initial and long-term moisture uptake (Figure 8).

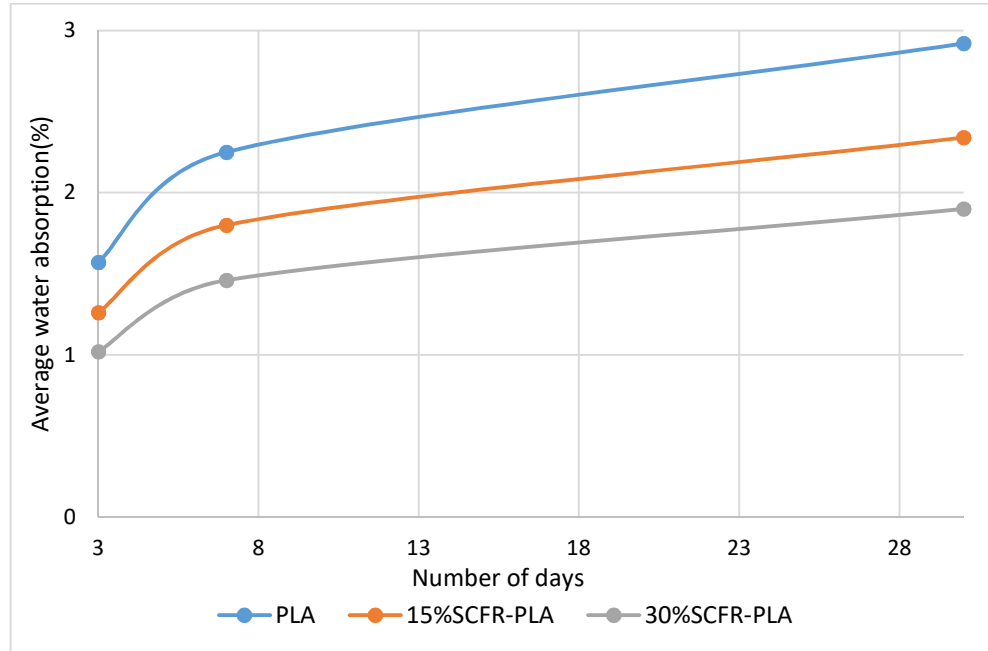


Fig. 8 – Moisture content over time

For PLA, the absorption rate between 3 and 7 days is 0.17% per day, the highest among all materials, before dropping to 0.029% per day between 7 and 30 days. In comparison, 15% SCFR-PLA exhibits lower slopes of 0.135% and 0.023% per day for the same periods, indicating reduced water penetration due to fiber reinforcement. The 30% SCFR-PLA samples show the lowest slopes, 0.11% and 0.019% per day, confirming that higher fiber content provides the greatest resistance to water absorption. All materials reach saturation at around 30 days, beyond which no further water uptake is observed, highlighting the stabilization of moisture content over time.

5. POROSITY OF SCFR-PLA

Porosity (P_t) is equal to pore volume (V_p) divided by total volume (V_t). It is expressed by the following equation:

$$P_t = \frac{V_p}{V_t} = \left(\frac{M_t - M_s}{M_t} \right) \quad (3)$$

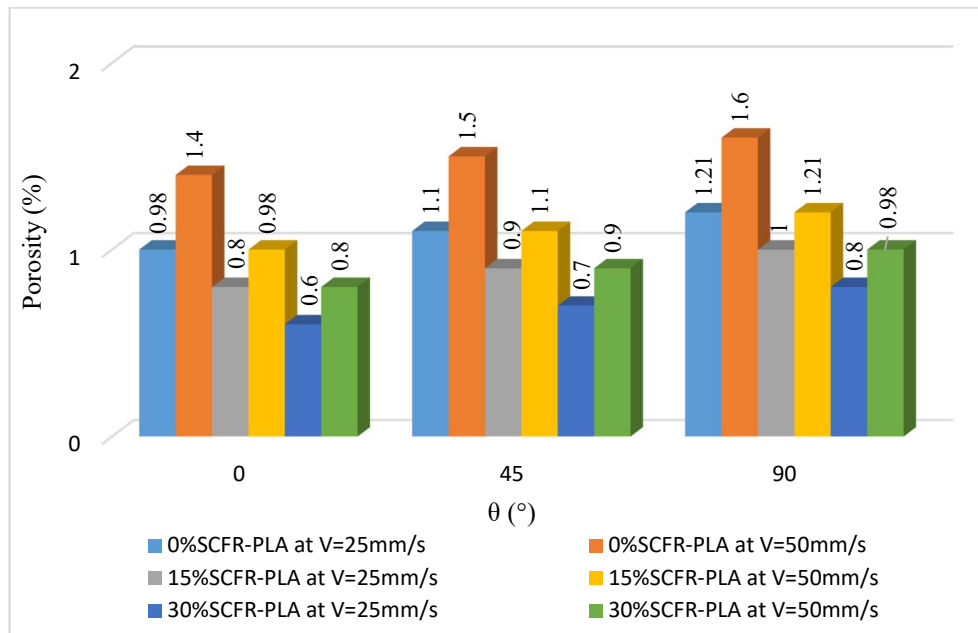


Fig. 9 – Influence of FDM parameters and materials on porosity.

Increasing the print speed from 25mm/s to 50mm/s leads to higher porosity levels, as the extruded filament has less time to fuse properly with adjacent layers, resulting in weaker interfacial bonding and more voids within the structure. The raster angle also plays a role, although its impact is usually moderate; different angles (0°, 45° and 90°) affect the overlap and continuity of deposition lines, which can alter the internal void distribution. Furthermore, incorporating carbon fibers into the PLA matrix tends to reduce porosity due to the space-filling effect of the fibers.

To validate the obtained results, the tensile fracture surfaces of the SCFR-PLA with %C=15% and %C=30%, printed at various speeds (V), were examined using Scanning Electron Microscopy (SEM) analysis. The corresponding SEM images are presented in Figure 10. A raster angle (θ) of 0° were considered in the analysis.

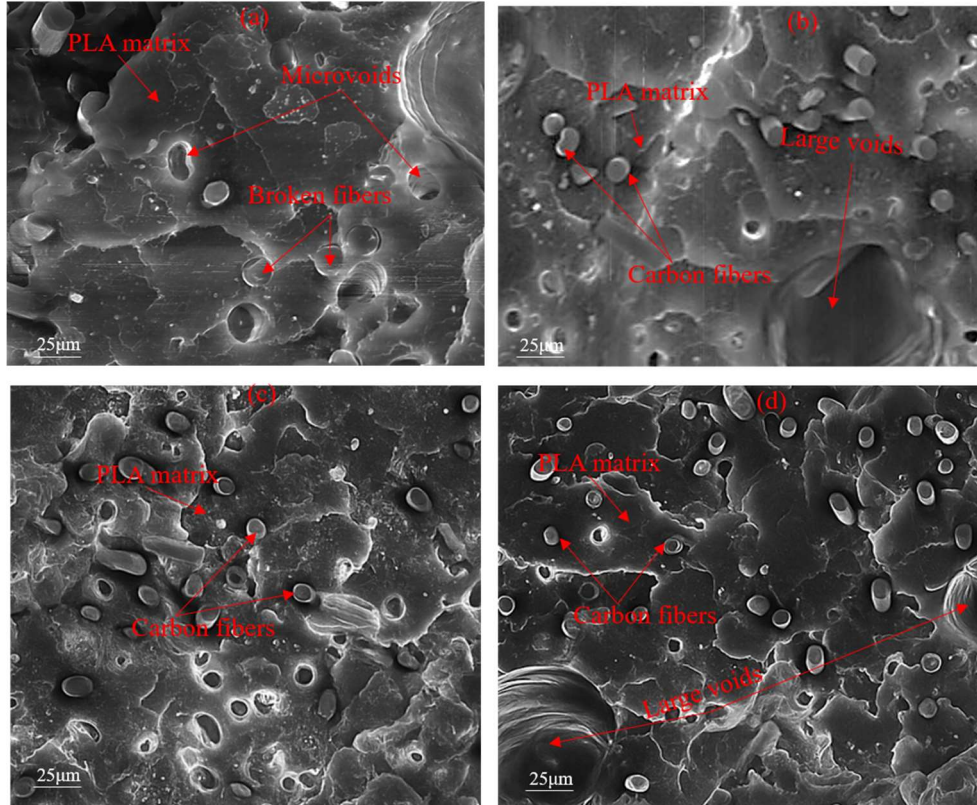


Fig. 10 – SEM images of the tensile damaged surfaces: (a) %C=15%, V=25mm/s. (b) %C=15%, V=50mm/s. (c) %C=30%, V=25mm/s. (d) %C=30%, V=50mm/s

It is clearly observed that increasing the printing speed (V) promotes the formation of extensive air pores, called large voids, within the material structure, which act as defects and significantly compromise the mechanical integrity of the printed parts. The higher speed limits the melting and consolidation processes, thereby reducing the mechanical strength and degrading the composite properties. Additionally, higher V may negatively affect interlayer adhesion, highlighting the importance of optimizing the trade-off between speed and print quality to achieve strong layer bonding.

6. CONCLUSIONS

This work investigated the relationships between mechanical, water absorption, porosity, and microstructural features in short carbon fiber reinforced polylactic acid (SCFR-PLA) composites printed by fused deposition modeling

(FDM), considering the coupled effects of printing speed (V), raster angle (θ), and fiber content (%C). The results show that stiffness (E) increases with %C but decreases with higher θ and V . Yield strength (YS) is inversely related to θ and %C, with V showing minimal influence. UTS decreases with θ but increases with V and %C. Ductility (ϵ_f) improves with V but decreases with θ and %C. Water absorption increased over time for all materials but was significantly reduced with higher %C, confirming the hydrophobic effect of carbon fibers. Pure PLA exhibited the highest uptake, while 30% SCFR-PLA showed the lowest, with all materials reaching saturation at around 30 days. Porosity analysis revealed that higher printing speeds tend to increase void formation, affecting mechanical performance. SEM analysis of tensile fracture surfaces for SCFR-PLA at $\theta=0^\circ$ revealed distinct differences between $V=25\text{mm/s}$ and $V=50\text{mm/s}$, highlighting the role of printing speed in fiber-matrix adhesion, pore morphology, and fracture mechanisms. Overall, the findings demonstrate that optimizing fiber content, raster orientation, and printing speed can significantly enhance mechanical performance, reduce moisture sensitivity, and control porosity in FDM-printed SCFR-PLA composites.

REFERENCES

1. H. Hentati, M. Dhahri, and F. Dammak, "A phase-field model of quasistatic and dynamic brittle fracture using a staggered algorithm," *J. Mech. Mater. Struct.*, **11**, 309–327 (2016). <https://doi.org/10.2140/jomms.2016.11.309>
2. Al. Nitu, V. Radu, L. Stoica, et al., "Characterization of the DHC crack parameters in zirconium alloys," *Romanian Journal of Physics*, **68**, 910 (2023).
3. Y. Kriaa, H. Hentati, and B. Zouari, "Applying the phase-field approach for brittle fracture prediction: Numerical implementation and experimental validation," *Mech. Adv. Mater. Struct.*, **29**(6), 828–839 (2022). <https://doi.org/10.1080/15376494.2020.1795957>
4. S. G. Bokuchava, P. Petrov, G. Genchev, et al., "Residual stress analysis in welded joints by neutron diffraction and computer modeling," *Romanian Journal of Physics*, **63**(7-8), 904 (2018)
5. B. Ben Fraj, T. Kamoun, H. Hentati, et al., "Optimization of forming force and Erichsen index using Taguchi design of experiments: Mathematical models and experimental validation," *Proc. Inst. Mech. Eng. Part B*, **238**(9), 1316–1326 (2024). <https://doi.org/10.1177/09544054231194107>
6. I. Messaoudi, B. Ben Fraj, H. Hentati, et al., "Phase transformations and electrothermal effects in EDM-machined steel: Surface topography, crater morphology, and debris evolution," *Romanian Journal of Physics*, **70**(7-8), 912 (2025). <https://doi.org/10.59277/RomJPhys.2025.70.912>
7. M. Popović, M. Pjević, A. Milovanović, et al., "Printing parameter optimization of PLA material concerning geometrical accuracy and tensile properties relative to FDM process productivity," *J. Mech. Sci. Technol.*, **37**(2), 697–706 (2023).
8. R.A. Badea, A. M. Voicu, A. Orian, et al., "From reconstructed DICOM images to 3D printed models: anthropomorphic dosimetric phantoms," *Romanian Rep. Phys.*, **76**, 804 (2024).

9. X. Wang, M. Jiang, Z. Zhou, et al., "3D printing of polymer matrix composites: A review and prospective," *Compos. Part B*, **110**, 442–458 (2017). <https://doi.org/10.1016/j.compositesb.2016.11.034>
10. A. V. Nastuta, F.D. Cojocaru, M. Ciolan, et al., "On the influence of atmospheric pressure plasma treatment on polyethylene terephthalate glycol filaments for 3D printing," *Romanian Rep. Phys.*, **76**, 404 (2024)
11. T. H. Le, V. S. Le, Q. K. Dang, et al., "Microstructure Evaluation and Thermal–Mechanical Properties of ABS Matrix Composite Filament Reinforced with Multi-Walled Carbon Nanotubes by a Single Screw Extruder for FDM 3D Printing," *Appl. Sci.*, **11**, 8798 (2021). <https://doi.org/10.3390/app11198798>
12. I. Ferreira, D. Vale, M. Machado, et al., "Additive manufacturing of polyethylene terephthalate glycol /carbon fiber composites: An experimental study from filament to printed parts," *Proc. Inst. Mech. Eng. Part L*, **233(9)**, 1866–1878 (2019). <https://doi.org/10.1177/1464420718795197>
13. A.P.G. Juan, V.S. Carlos, J.V.G. Luis, et al., "Structural composite based on 3D printing polylactic acid/carbon fiber laminates (PLA/CFRC) as an alternative material for femoral stem prosthesis," *J. Mech. Behav. Biomed. Mater.*, **138**, 105632 (2023). <https://doi.org/10.1016/j.jmbbm.2022.105632>
14. B. Sunil, A. Roberto, and J.G. Douglas, "Enhancing the interlayer tensile strength of 3D printed short carbon fiber reinforced PETG and PLA composites via annealing," *Addit. Manuf.*, **30**, 100922 (2019).
15. D. Stoof, K. Pickering, and Y. Zhang, "Fused Deposition Modelling of Natural Fibre/Polylactic Acid Composites," *J. Compos. Sci.*, **1(1)**, 8 (2017).
16. C. Vălean, L. Marşavina, M. Mărghiţaş, et al., "Effect of manufacturing parameters on tensile properties of FDM printed specimens," *Proc. Struct. Integr. Eng. Frac. Mech.*, **26**, 313–320 (2020). <https://doi.org/10.1016/j.prostr.2020.06.040>
17. S. Wang, L. Huang, S. Jiang, et al., "Microstructure evolution and tensile properties of as-rolled TiB/TAl5 composites with network microstructure," *Mater. Sci. Eng. A*, **804**, 140783 (2021).
18. C. Vălean, D.L. Stoia, C. Opreş, et al., "Effect of Fillers on Mechanical Properties of FDM printed PLA Components," *Proc. Struct. Integr.*, **56**, 97–104 (2024). <https://doi.org/10.1016/j.prostr.2024.02.043>
19. M.H. Hsueh, C.J. Lai, S.H. Wang, et al., "Effect of Printing Parameters on the Thermal and Mechanical Properties of 3D-Printed PLA and PETG, Using Fused Deposition Modeling," *Polymers*, **13(11)**, 1758 (2021). <https://doi.org/10.3390/polym13111758>
20. N. Maqsood, and M. Rimašauskas, "Characterization of carbon fiber reinforced PLA composites manufactured by fused deposition modeling," *Compos. C*, **4**, 100112 (2021). <https://doi.org/10.1016/j.jcomc.2021.100112>
21. H. Li, B. Liu, G. Lei, et al., "Mechanical performances of continuous carbon fiber reinforced PLA composites printed in vacuum," *Compos. Part B*, **255**, 109277 (2021). <https://doi.org/10.1016/j.compositesb.2021.109277>
22. I. Marcus, M. Garrett, C. Jason, et al., "Characterizing short-fiber-reinforced composites produced using additive manufacturing," *Adv. Manuf. Polym. Compos. Sci.*, **3(3)**, 81–91 (2017). <https://doi.org/10.1080/20550340.2017.1341125>
23. S. Ammar, B. Ben Fraj, H. Hentati, et al., "Mechanical performances of printed carbon fiber-reinforced PLA and PETG composites," *Proc. Inst. Mech. Eng. Part L J. Mater. Des. Appl.*, **238**, 1488–1499 (2024). <https://doi.org/10.1177/14644207231225761>

24. Z. Zhongsen, L. Yu, Y. Zhe, et al., "An investigation into printing pressure of 3D printed continuous carbon fiber reinforced composites," *Compos. A Appl. Sci. Manuf.*, **162**, 107162 (2022). <https://doi.org/10.1016/j.compositesa.2022.107162>
25. V. Mahesh, S.J. Athul, M. Vishwas, et al., "Investigation on the mechanical properties of additively manufactured PETG composites reinforced with OMMT nanoclay and carbon fibers," *Polym. Compos.*, **42(5)**, 2380–2395 (2021). <https://doi.org/10.1002/pc.25985>
26. R.T. Luiz Ferreira, I.C. Amatte, T.A. Dutra, et al., "Experimental characterization and micrography of 3D printed PLA and PLA reinforced with short carbon fibers," *Compos. Part B*, **124(1)**, 88–100 (2017). <https://doi.org/10.1016/j.compositesb.2017.05.013>
27. A.A. Ansari, and M. Kamil, "Effect of print speed and extrusion temperature on properties of 3D printed PLA using fused deposition modeling process," *Mater. Today Proc.*, **45(6)**, 5462–5468 (2021). <https://doi.org/10.1016/j.matpr.2021.02.137>
28. J. Nomani, D. Wilson, M. Paulino, et al., "Effect of layer thickness and cross-section geometry on the tensile and compression properties of 3D printed ABS," *Mater. Today Commun.*, **22**, 100626 (2019). <https://doi.org/10.1016/j.mtcomm.2019.100626>
29. K. Ajay, M.S. Khan, and S.B. Mishra, "Effect of machine parameters on strength and hardness of FDM printed carbon fiber reinforced PETG thermoplastics," *Mater. Today Proc.*, **27(2)**, 975–983 (2020). <https://doi.org/10.1016/j.matpr.2020.01.291>
30. F. Ning, C. Weilong, Q. Jingjing, et al., "Additive manufacturing of carbon fiber reinforced thermoplastic composites using fused deposition modeling," *Compos. Part B*, **80**, 369–378 (2015).
31. T. Kuncius, M. Rimašauskas, and R. Rimašauskienė, "Interlayer Adhesion Analysis of 3D-Printed Continuous Carbon Fibre-Reinforced Composites," *Polymers*, **13(10)**, 1653 (2021). <https://doi.org/10.3390/polym13101653>.